Article citation info:
Benkiewicz K. Modeling two-dimensional linear detonation engines with ANSYS Fluent package. Combustion Engines. 0000;XXX(X):xx-xx. https://doi.org/10.19206/CE-201364

Krzysztof BENKIEWICZ

Combustion Engines
Polish Scientific Society of Combustion Engines

Modeling two-dimensional linear detonation engines with ANSYS Fluent package

ARTICLE INFO

Received: 8 December 2024
Revised: 31 December 2024
Accepted: 12 February 2025
Available online: 10 March 2025

In this paper, a methodology for simulation of the Rotating Detonation Engines in ANSYS Fluent is developed. The overall approach relies on a 2D geometry, global reaction models of the homogeneous kerosene-air mixture, and appropriate boundary and initial conditions. It leads to the development and steady propagation of the detonation wave in a periodic channel. The wave structure and basic parameters are analyzed and compared to the data in the literature, as well as an ideal Chapman-Jouguet detonation. The trends of the detonation speed are analyzed for a range of equivalence ratios, mixture temperatures and pressures, mesh resolution and combustion models. The software is capable of simulation of complex phenomena occurring in the detonation wave. A cellular structure visible in real detonations can be predicted by CFD, although its scale differs due to the simplifications employed. The study shows that this methodology can be used for the analysis of propulsion systems operating on detonative combustion. It also indicates its limitations and areas for improvement. ANSYS's Fluent flexibility and user-friendly interface, combined with this methodology, help the user concentrate on R&D instead of coding.

Key words: *RDE, detonation, CFD, ANSYS Fluent, kerosene*

1. Motivation

Modern commercial and military aviation is realized by airplanes equipped with different propulsion systems: turboprops, turboshafts, turbojets and turbofan engines. Even though these machines differ in many aspects, they have many commonalities. All of them share a similar structure that includes compressor, combustor, and turbine. These machines work in accordance to the same Joule-Bryton cycle (see Fig. 1, Tsingas [20]), or its variation, where the compression is progressing along line 1–2, combustion at (almost) constant pressure along line 2–3, and expansion along line 3–4.

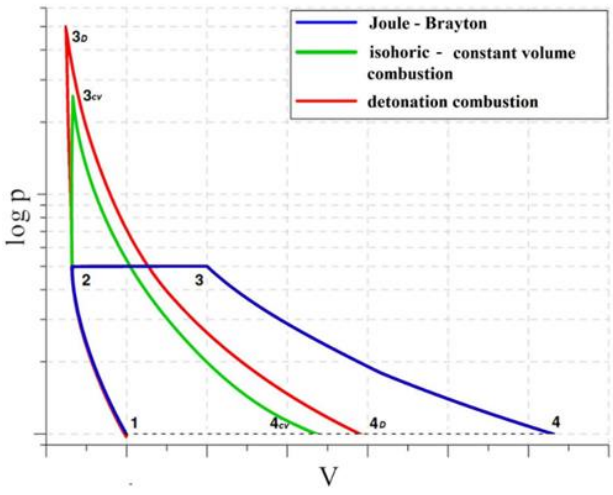

Fig. 1. Thermodynamic cycles of propulsion systems, Tsingas [20]

The Joule-Brayton cycle is not the most efficient as the thermal cycles with combustion at constant volume (with an increase of pressure) offer better theoretical performance. An example of such a cycle is the isobaric (Humprey) cycle. Even higher performance can be obtained (at least in theory) through the detonation (Fickett-Jacobb) cycle. Thus many scientific centers in the USA, Soviet Union/Russia, China, Japan, France and Poland have begun research on detonation and its practical application in propulsion systems (see, for example, Wolański [22–24], Xie [27], Nishimura [16]).

A very specific form of detonative propulsion is the Rotating Detonation Engine (aka RDE or CRDE, where "C" stands for "Continuous"), where the combustion wave travels in the cylindrical channel (hollow or annular) along its circumference at supersonic speed, while the fresh combustible mixture is continuously supplied along the channel axis (see Fig. 2, Tsingas [20]).

The pressure behind the detonation wave is much higher than upstream of the flame front, which results in higher combustion efficiency than the deflagration process used in traditional propulsion systems. At the same time, high speed and high pressure are the main difficulties in research on detonation engines. The classical deflagration-based combustor tests can be run for hours, provided that stable air and fuel supply are available. This technology is mature and has been mastered by several companies and research centers across the world. It is used in thousands of aircraft engines and power gas turbines. In contrast, the RDE technology is in the early development stage, at a low Technology Readiness Level (typically TRL < 6), and has several milestones to achieve. The detonation tests are usually short, with duration measured in seconds (see Wolański [25], Perkowski [17], Kindracki [11] or Kawalec [10]). The high speed of the detonation wave means that within these couple of seconds the combustion front and peak pressures pass around the RDE circumference several thousands of times. It is still a challenge to keep it stable for longer time, and the wave may transit through several different combustion modes (Perkowski [17]). The mechanism of these changes is unknown, the "safe" range of parameters are not defined, and the RDE operation control methods are still to

be developed. In parallel, very high turbulence level in the combustion chamber enhances heat transfer to the combustor walls significantly limiting its endurance. Measurement of the heat flux to the walls is a challenging task (see e.g., Kublik [14] and Meyer [15]). Heat flux to the walls is very high, thus active cooling methods are necessary to obtain sufficiently long engine operation tests. A 2 minute-long operation of the RDE was conducted only recently (NASA's Marshall Space Flight Center YouTube official channel [26]).

The tests of the RDE are the most important research methods. The literature is quite extensive. In many cases the fuel is gaseous hydrogen as the design of RDE is straightforward, the initiation is easy and reliable (Kawalec [9]). Other fuels under consideration are acetylene (Wolański [24]), methane, ethane, propane (Kindracki [11]) and kerosene (Perkowski [17]). Similar studies were also carried out in the USA (see, e.g. Knowlen [12]) and China (e.g., Zhou [31]).

Numerical simulations can give researchers insight into the internal structure of the detonation, the physical phenomena taking place at and downstream of the detonation front, and its dynamics and limitations. The academic communities rely mostly on in-house-developed codes where generations of researchers and PhD students spend years developing, implementing, debugging, modifying, debugging again, …, and use of their codes for scientific research. Commercial engine manufacturers have their own codes, too, but also turn their attention to commercial software. The lack of access to the source code is a disadvantage, but there is no need to develop and test numerical schemes, sub-models, Graphical User Interface (GUI), and post-processing procedures, which is a strong advantage of commercial codes. With commercial CFD software the user can concentrate on design and technology development, not on software coding and debugging. A commercial code with a well-defined methodology is often good enough for R&D.

Various research teams build their own CFD methodologies which share some commonalities and differ in some aspects. It is hard to find a complete methodology in the literature. The little things that are not reported often make a difference between good and bad models. In this paper development of methodology for numerical simulation of the simple linear RDE using ANSYS Fluent is summarized. It can be used by the scientific and engineering community for the development of their own models.

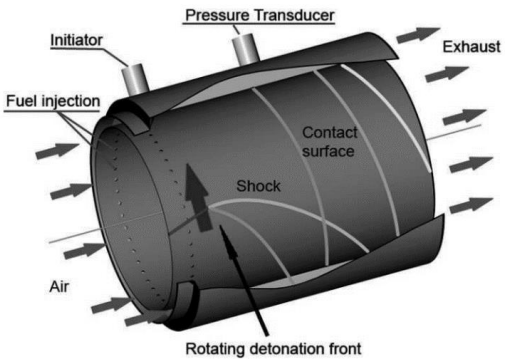

Fig. 2. Schematic view of rotating detonation engine, Tsingas [20]

2. Numerical model and CFD code

In this paper, a linear detonation engine running on a gaseous mixture of kerosene vapor and air is considered. The fuel and oxidizer/air injection, fuel evaporation and mixing process are omitted here assuming that it takes place upstream of the combustion zone. A two-dimensional rectangular domain represents a flat combustor with an inlet and outlet on two opposing sides of the domain and periodic boundary conditions on the remaining pair of edges. Such a model is intended for rapid development of methodologies that later on will be used in complex three-dimensional geometries of more realistic combustor designs. The simplicity should result in low development costs and fast turn-around time. Specifically, the 2D model could be used to evaluate the impact of boundary conditions, operating conditions, equivalence ratios, chemical reaction models, etc., on the development, propagation and stability of the detonation wave, its speed, and detailed structure and dynamics of the detonation front. A separate study could be done do find out optimal model and solver settings, as well as initialization methods.

2.1. Combustor geometry and mesh

The schematic view of the combustor geometry is presented in Fig. 3. The combustor is W = 452 mm wide and L = 100 mm long. The combustible mixture of air and kerosene vapour enters the domain through the top long edge marked as the "inlet" and leaves it through the bottom long edge marked as an "outlet". The detonation wave is supposed to propagate in the direction perpendicular to the inlet/outlet boundaries. Periodic boundary conditions applied to the left and right edges allow for continuous propagation of the wave, which, after reaching one end of the domain, leaves it and re-enters again from the other side of the domain. The domain is covered with a uniform coarse quad mesh of the size of 904 × 200 cells in the horizontal and vertical directions, respectively. The cell size is 0.5 × 0.5 mm.

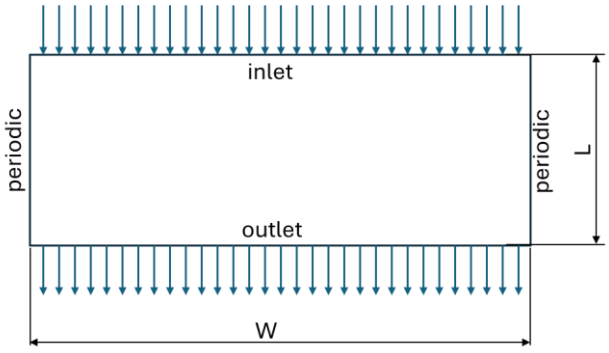

Fig. 3. Computational domain

It is important to note that the domain size was selected arbitrarily and should not be treated as an unfolded cylindrical geometry. Even though some papers suggest that such manipulation is possible, it relies only on the similarity of both flat (planar) and unfolded cylindrical solutions, but the equations of fluid motion are different in cartesian and cylindrical coordinate systems. An example of such an approach can be found, e.g., in Davidenko [3], where it was

assumed that the channel height is small compared to the radius and that parameter variation in the radial direction can be omitted. The authors did not quote the equations nor coordinate system used, but the term "2D planar geometry" suggests such an assumption.

One should also remember that the assumed length of the domain is actually a constraint applied to the model. It defines the linear periodicity of the detonation wave, which may be and usually is different than the periodicity obtained in an infinitely long channel, should multiple detonation waves be predicted by such a model.

2.2. Governing equations and combustion model

The selected governing equations of fluid motion are the Euler equations of homogeneous (gas-only) multi-component reacting mixture, so the inviscid model is selected in the ANSYS Fluent options panel. This popular simplification comes from the model's lack of solid walls and being run on a relatively coarse mesh. Thus, the terms representing viscous forces and species diffusion are expected to be small compared to other terms in the Navier-Stokes equations. The set of Navier-Stockes equations is described in ANSYS Fluent Theory Guide [1] (Chapter 1, Section 1.2 and following sub-sections), but they are dispersed into a few paragraphs, so they are sometimes difficult to read. For completeness, these equations can be converted to the conservative vector form as follows:

$$\frac{\partial U}{\partial t} + \frac{\partial F}{\partial x} + \frac{\partial G}{\partial y} = Q \tag{1}$$

where U, F, G and Q are vectors:

$$U = \begin{bmatrix} \rho \\ \rho_i \\ \rho \cdot u \\ \rho \cdot v \\ \rho \cdot E \end{bmatrix} \tag{2}$$

$$F = \begin{bmatrix} \rho \cdot u \\ \rho_i \cdot u \\ \rho \cdot u^2 + p \\ \rho \cdot u \cdot v \\ (\rho \cdot E + p) \cdot u \end{bmatrix}, G = \begin{bmatrix} \rho \cdot v \\ \rho_i \cdot v \\ \rho \cdot u \cdot v \\ \rho \cdot v^2 + p \\ (\rho \cdot E + p) \cdot v \end{bmatrix}, Q = \begin{bmatrix} 0 \\ \dot{\omega}_i \\ 0 \\ 0 \\ 0 \end{bmatrix}$$

ρ is the mixture density, ρ_i is the i-th specie density, i = 1, …, n–1, n is the number of species, and u and v are velocity components in x and y direction, respectively. p is static pressure, and E is total specific energy of the mixture defined as:

$$E = \sum_{i=1}^{i=n} \left(\int_{298.15}^{T} y_i \cdot c_{pi} \cdot dT \right) - \frac{p}{\rho} + \frac{(u^2+v^2)}{2} \tag{3}$$

where T is the static temperature of the mixture, y_i is the i-th species mass fraction, and c_{pi} is the i-th species-specific heat at constant pressure. Specific heats are described by polynomial functions of temperature as the temperature range in RDE may span thousands of Kelvin.

The methodology developed here is used in CFD analysis of the detonation wave propagating in a mixture of regular aviation fuel (kerosene) and air, as this fuel and oxidizer are commonly used in contemporary aviation. The concept of wide application of future fuels like synthetic jet fuel or sustainable aviation fuels (SAF) is emerging now but is not considered in this paper. Liquid hydrogen or methane in aviation is an option for an even more distant future.

The kerosene or Jet-A fuel is a mixture of various structures, lengths, and molecular mass hydrocarbons. The full combustion model would include hundreds of species and thousands of reactions and would be computationally very expensive. Much simpler models are being used for research purposes, providing reasonable results within affordable cost and time. This study's mixture consists of just 6 species: kerosene vapour (represented by $C_{12}H_{23}$), O_2, CO_2, H_2O, and N_2. The species density and mixture density meet the following equation:

$$\rho = \sum_{i=1}^{i=n} \rho_i \tag{4}$$

thus the i-th specie mass fraction is defined as:

$$y_i = \frac{\rho_i}{\rho} \tag{5}$$

The last specie is the most abundant specie (N_2), and its partial density is calculated from:

$$\rho_n = \rho - \sum_{i=1}^{i=n-1} \rho_i \tag{6}$$

The continuity, momentum and energy equations (2) are accompanied by the ideal-gas equation of state:

$$\frac{p}{\rho} = \frac{R}{M} \cdot T \tag{7}$$

where M is the molar mass of the mixture and R is the universal gas constant.

The term $\dot{\omega}_i$ in equation (2) is the i-th specie source/sink term due to chemical reactions. Chemical reaction of kerosene and oxygen is described by one-step global reaction mechanism:

$$C_{12}H_{23} + 17.75\ O_2 \rightarrow 12\ CO_2 + 11.5\ H_2O \tag{8}$$

This reaction can proceed if the temperature is higher than 350 K to avoid numerically-driven autoignition. The reaction rate is governed by the Arrhenius-type equation:

$$k = A \cdot \exp\left(\frac{-E_A}{R \cdot T}\right) \tag{9}$$

where k is the reaction rate, A = $2.587 \cdot 10^9$ is the pre-exponential factor, and $E_A = 1.005 \cdot 10^8$ J/kmol is the activation energy. For one-step irreversible reaction (8), the fuel (kerosene) sink rate is calculated from:

$$\dot{\omega}_{C_{12}H_{23}} = -M_{C_{12}H_{23}} \cdot k \cdot [C_{12}H_{23}]^{0.25} \cdot [O_2]^{1.5} \tag{10}$$

where $M_{C_{12}H_{23}}$ = 167 kg/kmol is the molar mass of kerosene and square brackets indicate molar concentration of species. The production/consumption rate of other species is related to (10) through molar ratios between reactants and products in equation (8). Nitrogen is treated as an inert specie and does not take part in the reaction. The combustion model described above is a modified version of the default kerosene-air combustion model provided in ANSYS Fluent package where the activation energy E_A is slightly reduced (by ~20%) from original model to facilitate initiation of the detonation. With the original value of E_A the detonation was not developing for given coarse mesh and 2D model.

In the literature, one can find more sophisticated models. Example schemes can be found in Westbrook [21], Dagaut et al. [2], Gerasimov [6, 7], Zheng [29], Zettervall [30], Strelkova [19] or Franzelli [5]. They include more species and radicals and are expected to reproduce better chemistry of the reacting system. The two-step reaction model will be considered in this paper later on, but other models include more species and equations and are computationally more expensive than Eq. (8). Some of them will be tested in the future once some kind of "best practice" for RDE modelling is developed using simpler models.

2.3. Boundary and initial conditions

The selection of the "right" boundary conditions for the model is critical to have the model working properly, especially when access to the source code is limited. ANSYS Fluent offers several options here, including velocity-inlet, pressure-inlet and mass-flow-inlet boundary conditions. The objective is to apply the boundary conditions that will allow for the development of the detonation wave. After some trial tests, the mass-flow-inlet boundary condition is applied along the top long edge of the domain was selected. With this approach, it is assumed that the overall fuel and air flow rate is not impacted by the detonation wave, but local parameters at the inlet boundary can vary, especially if the detonation front is "attached" to the inlet. In this situation, the high pressure behind the detonation wave blocks or reduces incoming flow, and this "missing" inflow is pushed through parts of the inlet away from the detonation wave front. The bottom edge of the domain is modelled as a reflecting pressure outlet with a predefined temperature and composition for the mixture, should the backflow into the domain occur during analysis. The backward inlet temperature is set to 3000 K, and the composition is set to products of perfect combustion according to Eq. (8). In "normal" operation, the backflow should not occur.

For the baseline model, the incoming stoichiometric kerosene-air mixture is assumed with the pressure of p = 1 bar and an initial static temperature of T = 300 K, flowing perpendicularly to the boundary at v_y = –150 m/s. The y-axis is pointing up, so the incoming going flow from top to bottom has a negative value of the v_y velocity component. The inlet mass flow rate for these conditions is about 82.8 kg/s (2D model assumes 1 m "depth" of the domain). The top 5% of the domain next to the inlet boundary condition is filled with the fresh incoming mixture, while the remaining bottom 95% is filled with the products of kerosene-air (perfect) combustion. The detonation is initiated by a small patch of high temperature (T = 1500 K), high pressure (p = = 150 bar) and high x-velocity (v_x = 1500 m/s) located in the bottom 95%-zone of the computational domain (see Fig. 4). The parameters are selected arbitrarily by trial and error and represent conditions created by the local pyrotechnical device used in many experiments. Its objective is to directly initiate the propagation of the detonation. The impact of initial conditions and initiation patch is diminished once the wave traverses the domain a couple of times.

The reason behind the choice of initial and boundary conditions was to obtain a steady propagating detonation wave in a given mixture, as the reproduction of realistic initiation of the detonation process in such a simple model is difficult. The deflagration-to-detonation transition (DDT), which is a challenge for numerical analysis (see Dziemińska [4]), is thus omitted.

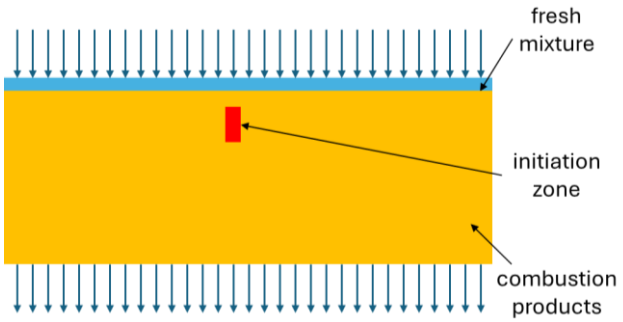

Fig. 4. Initial conditions

2.4. Numerical method

All the models shown in this paper are calculated using ANSYS Fluent 2023 R2 in double-precision mode. The package provides several solvers for various flow problems. The cases analyzed in this paper are run using always the same methods. The density-based solver is selected with implicit formulation and Roe-FDS flux type definition. Spatial discretization of gradients is last-square-cell-based, flow equations are discretized using 2^{nd} order upwind methods and temporal discretization is implicit 2^{nd} order. A "High Speed Numerics" option is turned on to set other solver settings to "optimal" levels as recommended by ANSYS. The chemistry is solved using "Stiff" solver. The variable time step is calculated based on Courant number set to 2.5, and up to 30 sub-iterations are calculated per each time step. The variable time step is typically of the order of $3 \cdot 10^{-7}$ s.

3. Results and discussion

3.1. Base case

Figures 5–8 show the position of the detonation wave in the domain and structure of the flow field for the base case at the time t = 3 ms. The black vertical and horizontal lines and arrows seen in Fig. 5 indicate lines along which profiles of the flow field properties are plotted on figures shown later on in this paper. The overall structure of the detonation front is typical, as has been shown in several other publications (see Hishida [8] or Yi [28]). The detonation front is attached to the inlet boundary. It is slightly curved and smeared, as the mesh resolution is not very high (see Fig. 6).

The structure of the flow field is a classical one, including the detonation wave itself, the shock wave propagating in the combustion products, the contact surface following the shock wave, and the deflagration wave separating incoming fresh mixture and post-deflagration combustion products. The coarseness of the mesh does not allow for the full development of the Kelvin-Helmholtz-like vortex structure in the contact surface often visible in similar simulations. Nevertheless, it is sufficient to show weak expansion waves behind the detonation front. These features would be much better resolved if the cell size was much smaller than 0.5 mm. Higher initial mesh density and/or Adaptive Mesh Refinement (AMR) would be very helpful here.

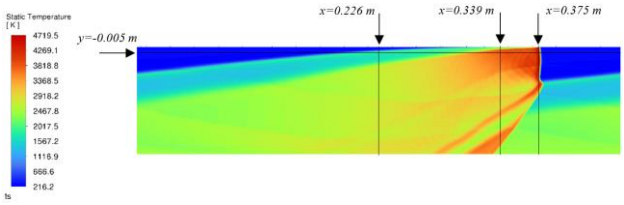

Fig. 5. Temperature distribution at t = 3 ms

Fig. 6. Pressure distribution at t = 3 ms

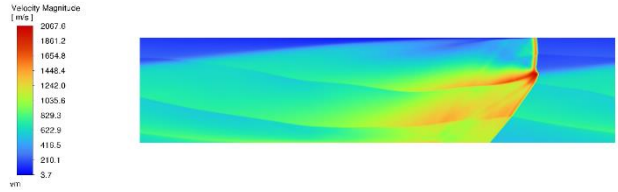

Fig. 7. Velocity magnitude distribution at t = 3 ms

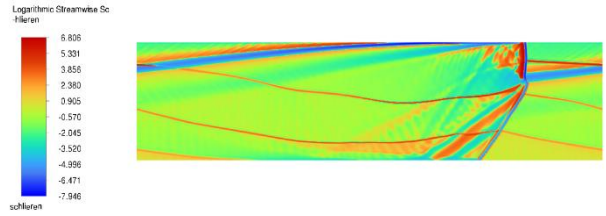

Fig. 8. Logarithmic streamwise Schlieren (density gradient) distribution at t = 3 ms

Interesting features are visible in Fig. 7 and 8. Figure 8 presents Schlieren-like plot indicating areas of high density gradients. One can notice several lines stretching between periodic boundary conditions. These lines point out on more interactions of the detonation wave with other flow phenomena and boundary conditions. The origins of these lines can be found in the initiation and development of the detonation process. After the beginning of the calculations, the relatively weak shock waves emanate from the initiation zone and propagate through the domain. Slightly stronger shock propagates to the right (due to high positive x-velocity mapped in the initiation zone), and weaker shock waves propagate in the opposite direction. These stronger waves do not create the detonation wave until they collide with the inlet boundary. The interaction of the stronger shock with the inlet boundary conditions results in a local increase of pressure and temperature behind the reflected shock wave. This hot spot is then an actual initiation of the detonation wave front, attached shock wave downstream of it, and deflagration behind it. This mechanism is common to all the models, and the failure of the detonation wave development only happens if this reflection from the inlet is too weak. The wave is allowed to propagate for a physical time long enough to allow for several passes through the domain and wash out initial conditions. Since the domain is periodic, the detonation wave catches with the deflagration wave. The point of contact is a source of shock wave and contact discontinuity. Such a flow structure of the detonation wave, shock wave and contact discontinuity propagates to the right.

In parallel to the process mentioned above weaker left-propagating shocks reach the pressure outlet and meet the upcoming right-propagating shock wave. This results in minor disturbances. The contact discontinuity also reaches the pressure outlet boundary, and initially, its reflection from the outlet seems very weak but gains strength far downstream of the initial contact with the outlet boundary. The passing shock wave makes it stronger and enhances its propagation upstream. After the next two passes of the detonation wave through the domain, this reflected post-contact-discontinuity wave reaches the detonation front and interacts with it. Thus, the flow structure becomes much more complicated than in many simulations shown in the literature. The details of the detonation front are shown in zoom-in Fig. 9–13.

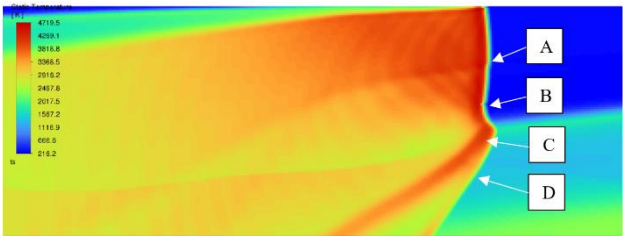

Fig. 9. Temperature distribution within the detonation front (zoom-in) at t = 3 ms

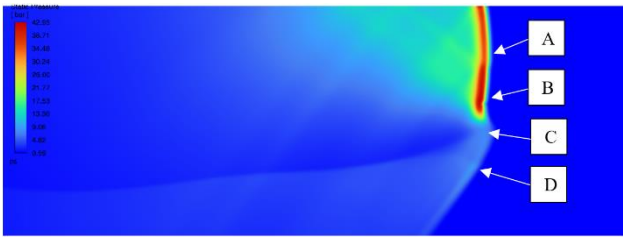

Fig. 10. Pressure distribution within the detonation front (zoom-in) at t = 3 ms

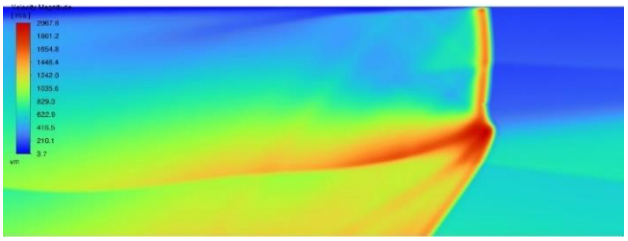

Fig. 11. Velocity magnitude distribution within the detonation front (zoom-in) at t = 3 ms

More insight into the flow field structure is shown in Fig. 13, where the velocity vectors colored by gas temperature are plotted on top of the contour lines of static pressure. For image clarity, only every 5th vector is plotted. The overall flow structure is similar to the results published by Hishida [8] and Yi [28]. The velocity vectors just behind the detonation wave are pointing to the right (as expected),

but there are two expansion waves: one weaker emanating from the inlet boundary and the second, slightly stronger, from the point of collision of the detonation wave and the deflagration wave. The latter propagates toward the inlet and the velocity vectors behind the front of this wave turn more toward the outlet. It is enhanced by the "reflected post-contact-discontinuity wave" mentioned above.

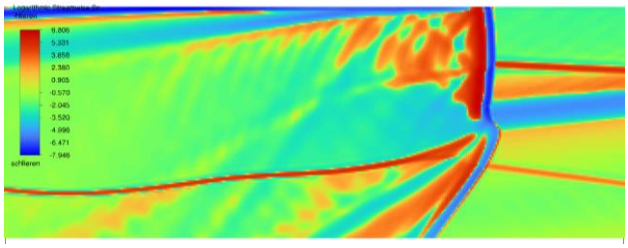

Fig. 12. Logarithmic Streamwise Schlieren (density gradient) distribution at t = 3 ms

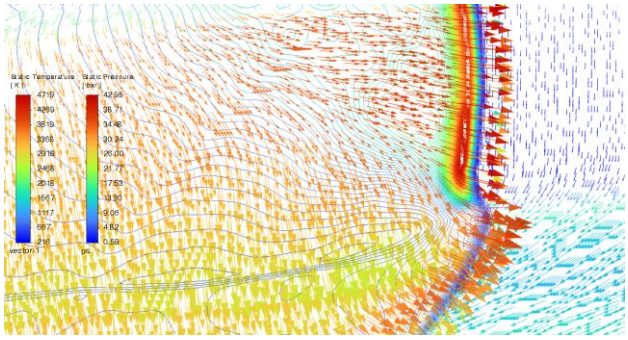

Fig. 13. Velocity vectors colored by gas temperature on top of velocity magnitude contour lines at t = 3 ms

3.2. Base case – detonation wave structure

The 2D plots present well overall structure of the detonation wave. More insight can be gained by analysis of profiles of various flow field parameters taken along the horizontal and vertical black lines marked in Fig. 5. The centre of the cartesian coordinate system is located in the top left corner of the domain with the x-axis pointing to the right and the y-axis pointing. Figure 14 shows the profiles of pressure, temperature, velocity components and main species along the horizontal line located at y = –0.005 m downstream of the inlet. Figures 15–17 show similar profiles taken along vertical lines located at x = 0.375, 0.339 and 0.226 m from the left boundary of the domain, so from the one that is the closest to the detonation wave to the line far away downstream of the detonation wave. In all the plots, the profile of pressure is shown to facilitate the relative location of various features on all the profiles.

Starting from the right side of the plots shown in Fig. 14, the detonation wave is clearly visible as a sharp peak in pressure profile with a max value of 36.48 bar located at x = ~0.376 m, even though it is smeared across ~4–5 cells. The temperature peak follows the pressure with a max value of 4471 K located ~1 mm (2 cells) behind the pressure peak. Of course, the max temperature is overestimated because of a simplified combustion model without radicals like CO, OH, H and pollutants NO_x. As one moves to the left from the pressure peak, both profiles drop down behind the detonation wave to the post-detonation conditions, visible as an almost flat region ending at x = ~0.348 m. At this point, the behavior of the temperature and pressure profiles changes. The pressure continues its steady drop as the flow is expanding until it reaches about 0.86 bar. The temperature and the concentration of the combustion products (CO_2 and H_2O) drop quickly from x = ~0.348 m to x = ~0.285 m, indicating a transition from the post-detonation to the post-deflagration region. The latter extends from x = ~0.225 m to x = ~0.285 m. The temperature behind the deflagration front is visibly lower than behind the detonation front. Also, not all the fuel is burnt with the mass fraction reaching y_{C12H23} = ~0.0005.

The fuel consumption behind the detonation wave is complete. The small temperature depression is the effect of the flow expansion and local gas acceleration. The x-velocity profile indicates expansion as the gas moves in the opposite direction from the gas just downstream of the detonation wave. Finally, at x = ~0.200 m, the temperature and combustion product mass fraction drop again when the profile line crosses the region of the unburned incoming mixture.

As it was written before the applied boundary conditions impose the total airflow. If part of the inlet is blocked by the detonation wave and the high-pressure post-detonation region, then the blocked air-fuel mixture is forced to flow through areas away from the detonation wave with a velocity higher than the assumed 150 m/s and static pressure lower than the assumed 1 bar. The blockage is located only in the close vicinity of the pressure peak with relatively low inflow y-velocity just behind it. The y-velocity does not reach zero on the plot as the profile line is slightly downstream of the inlet and where the impact of the blockage is already reduced.

Figure 15 shows the profiles of pressure, temperature, species concentration (H_2O, CO_2, O_2) and velocity components taken along the vertical line at x = 0.375 m so just downstream of the detonation wave front. Important: The horizontal axis marked as "y [m]" in Fig. 15–17 shows the distance from the inlet boundary condition. Fuel concentration is omitted as it drops to zero almost immediately downstream of the inlet. The first peak of pressure is located at the inlet and is followed by a "valley" and the second pressure peak. The "pressure valley" is the effect of the curvature of the detonation wave and the larger distance of the profile line from the detonation front at its center (point "A" in Fig. 9 and 10), while the second pressure peak is located where the profile line crosses the detonation front again (point "B"). The plateau between y = 0.034 m and y = = 0.044 m, so after the second peak, is the contact discontinuity (point "C"), and it is followed by the shock wave seen as a sudden drop of pressure to p = ~0.84 bar (point "D"). The pressure then slowly increases to p = ~0.97 bar at the outlet. The temperature downstream of point "D" decreases in the post-deflagration zone and, at x = ~0.065 m, increases again and stabilizes at the value representing the post-detonation combustion products. The kink in the temperature and velocity profiles is associated with the "reflected post-contact-discontinuity wave" mentioned above.

The analysis of profiles in the plateau region indicates the presence of a W-shaped y-velocity profile and Λ-shaped

x-velocity profile. The middle peak of y-velocity profile and peak of x-velocity profile are located in the contact discontinuity area (smeared due to low mesh resolution). The two valleys in y-profile are located between the post-detonation zone and contact discontinuity, and between the contact discontinuity and the shock wave. The boundaries between these three will eventually lead to development of vortices. These vortices will have opposite directions of rotation and different strength and finally merge into a Kelvin-Helmholtz-like instability. Clearly a model with better resolution in this area is needed to get better insight in the details of the flow filed in this area.

The profiles shown in Fig. 16 present the same parameters taken along the vertical line located further behind the detonation wave. The pressure just downstream of the inlet is quite high (p = ~13 bar) but not sufficient to immediately detonate the incoming mixture. The temperature is rising quickly as the line enters the post-deflagration zone reaching the peak at y = ~0.004 m, where the post-detonation zone begins. The impact of the "reflected post-contact-discontinuity wave" crossing detonation wave is visible as a small kink in temperature profile at y = ~0.023 m. The y-velocity and pressure drop until y = ~0.045 m, where the post-detonation zone ends. Again, the line enters the post-deflagration zone, but this time is affected by the oblique shock wave and contact discontinuity. This change has the form of a weak shock wave (pressure increase from 2.7 to 4.6 bar). This high-pressure zone contains contact discontinuity visible as x-velocity and temperature peak at y = ~0.064 m. At the same time, the y-velocity reaches a local maximum, and the gradients of the velocity components will eventually lead to the development of vortices further downstream. The concentration of the products in the zone between y = = ~0.045 m and y = ~0.076 m is lower than behind the detonation wave because this region is created from the post-deflagration combustion products compressed by the shock wave emanating from point "D" (Fig. 9 and 10). The next region, between y = ~0.076 m and the shock wave at y = = ~0.093 m, is a zone of compressed post-detonation products.

Finally, the last profiles taken along the vertical line at x = 0.226 m are shown in Fig. 17. The pressure profile shows 2 shock waves at y = ~0.048 m and y = ~0.085 m. Both are caused by the "reflected post-contact-discontinuity wave" propagating toward the inlet. Its impact on the profiles is much stronger than at x = 0.339 m, and as far downstream of the detonation wave, the pressures are much lower than closer to the detonation front. The temperature and species concentration profiles split the profiles at y = = ~0.016 m into two zones: the post-deflagration and the post-detonation. The transition from one zone to the other is smeared over several points partially because of the coarseness of the mesh and partially because of mixing (numerical diffusion) taking place behind the detonation front.

Among the key parameters describing the detonation phenomena is the detonation wave velocity. In order to estimate its value as predicted by the CFD model a "pressure gauge" is placed in the domain to "monitor" pressure and record passes of the detonation wave. Figure 18 shows recorded pressure at the "gauge" vs. time. As one can notice, the wave needs about 3–4 passes with the peak pressure variation of the order of 30–40 bars before it becomes quasi-stable. Once the wave is stable, the variation of peak pressure drops below 10 bars. For the known length of the domain, the time difference between the peaks gives the wave speed equal to 2176 m/s, based on the last 6 passes of the wave (see Fig. 19). For $\phi = 1$ the ideal detonation wave velocity (Chapman-Jouguet velocity, CJ) calculated by the STANJAN code (see Reynolds [18] for details) is equal to 1789 m/s.

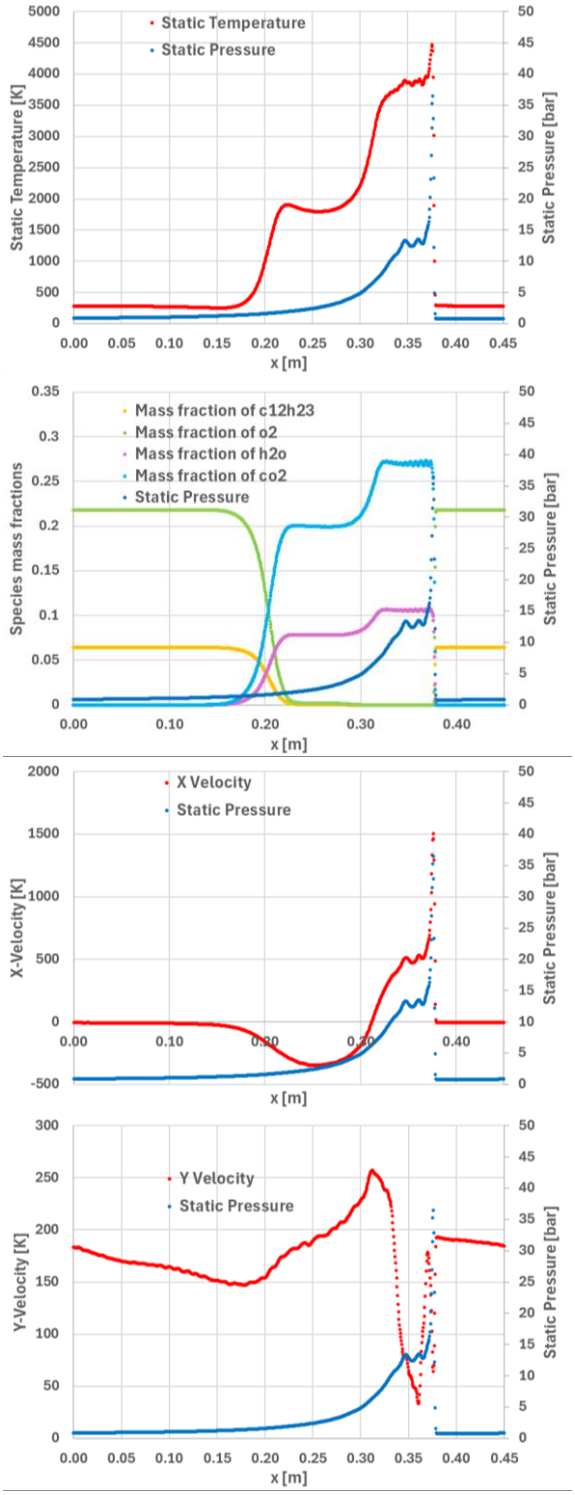

Fig. 14. Profiles of pressure, temperature, main species concentrations, and velocity components along horizontal line at y = –0.005 m downstream of inlet at t = 3 ms

Thus, the CFD model predicts about 21% higher detonation wave speed than the theoretical CJ value. The main reason behind this difference is the over-simplified combustion model, which assumes CO_2 and H_2O are the only combustion products. The STANJAN code predicts that combustion products may also contain CO, OH, H and NO_x, as well as minor traces of other species. Modified activation energy has virtually no impact on the detonation wave velocity obtained from the CFD models.

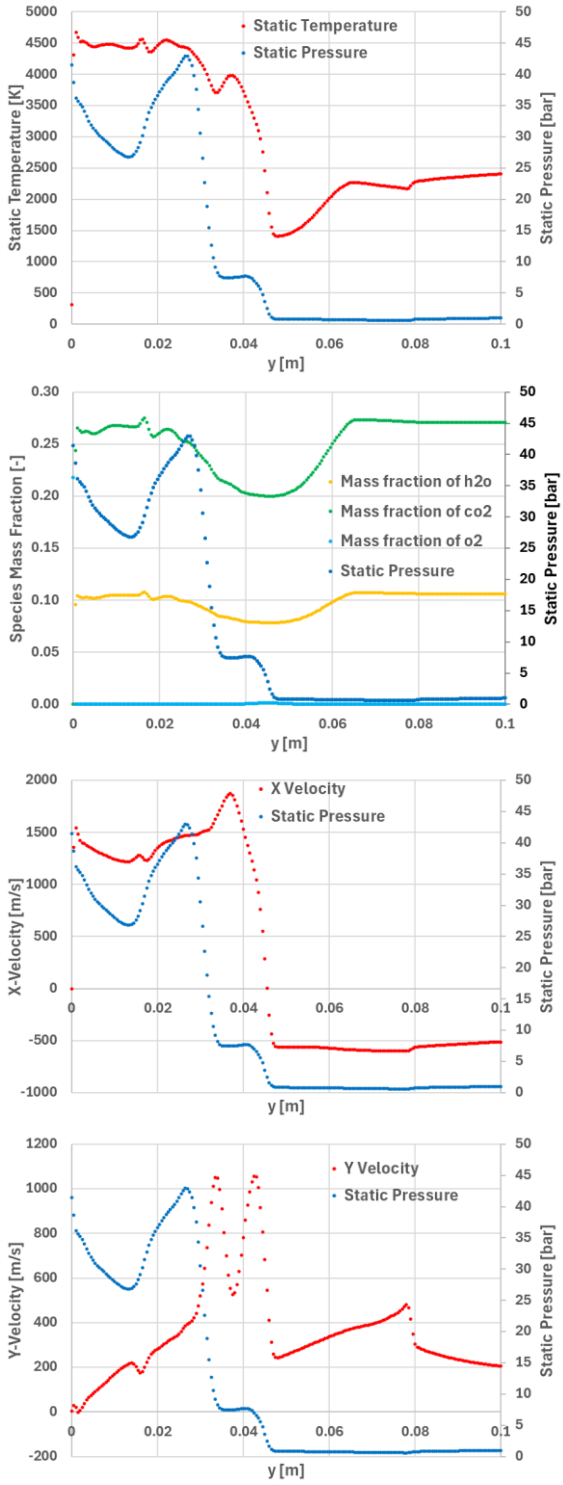

Fig. 15. Profiles of pressure, temperature, main species concentrations, and velocity components along vertical line at x = 0.375 m (see Fig. 5) at t = 3 ms

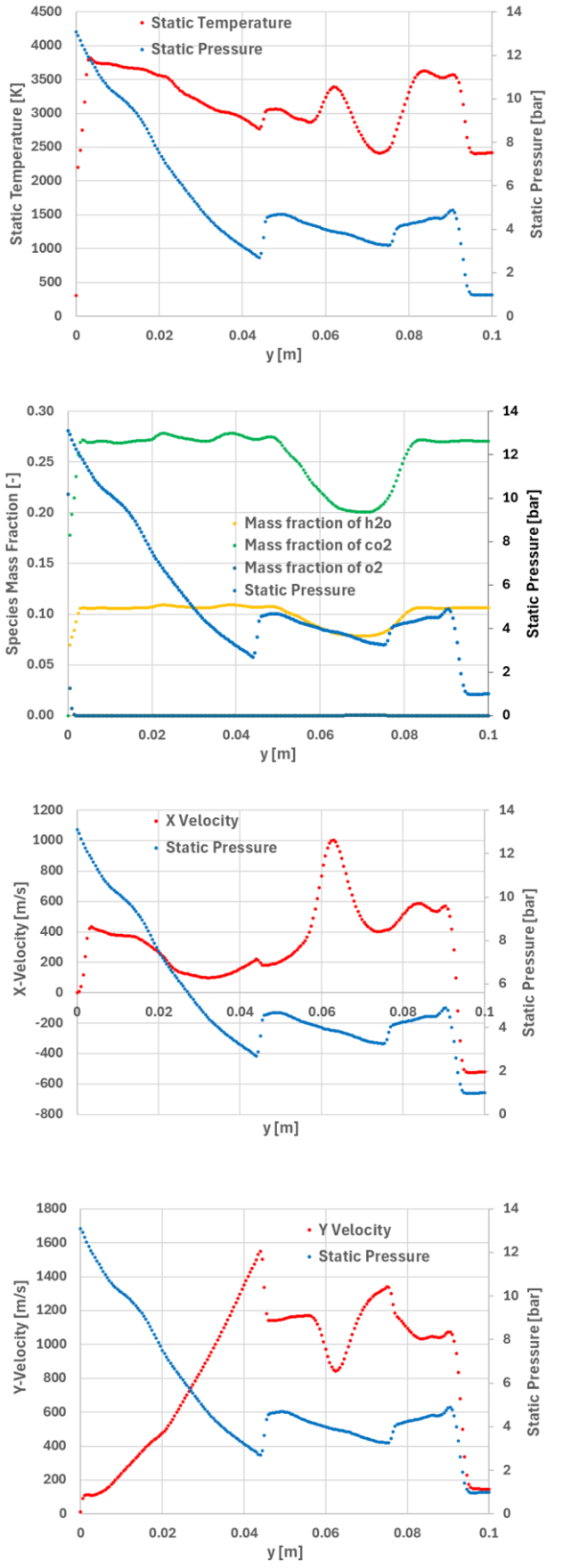

Fig. 16. Profiles of pressure, temperature, main species concentrations, and velocity components along vertical line at x = 0.339 m (see Fig. 5) at t = 3 ms

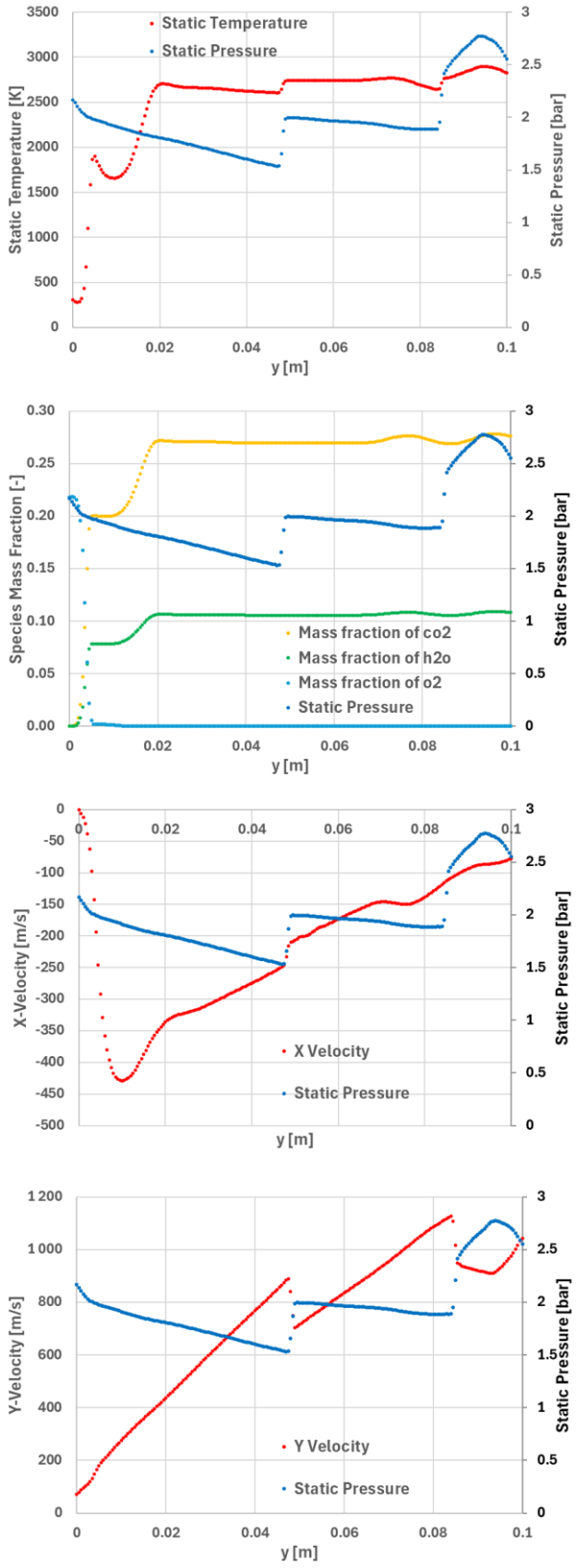

Fig. 17. Profiles of pressure, temperature, main species concentrations, and velocity components along vertical line at x = 0.226 m (see Fig. 5) at t = = 3 ms

3.3. Parametric study

Several analyses are performed for a wider range of parameters like equivalence ratios (Fig. 20), temperatures (Fig. 21) and pressures (Fig. 22). The CFD model predicts a very similar trend of detonation wave speed vs. equivalence ratio with a slight shift of the peak velocity to higher equivalence ratios in the STANJAN simulations. This may be related to the change in the composition of the combustion products for higher equivalence ratios. The dependence on inlet temperature shows a small drop in the detonation velocity with an increase in inlet temperature or pressure in both CFD and STANJAN calculations. In all the simulations, CFD tend to overpredict the detonation wave velocity. It becomes obvious that a combustion model with more reactions and reactants, e.g., CO and OH, needs to be applied.

3.4. Two-step combustion model

A two-step kerosene combustion model was proposed by Franzelli [5]. The fuel surrogate is $C_{10}H_{20}$, so the stoichiometry is slightly different from that of the base case. The reaction consists of 2 steps:

$$C_{10}H_{20} + 10\ O_2 \rightarrow 10\ CO + 10\ H_2O \quad (11)$$

$$CO + 0.5\ O_2 \leftrightarrow CO_2 \quad (12)$$

The first reaction is fast and irreversible, the second is slow and reversible. The reaction rate coefficients are described in Frenzelli [5] and are copied into ANSYS Fluent without any modifications. The correcting factors dependent on equivalence ratio ϕ are equal to 1 for ϕ smaller than 1 and thus could be omitted for base case. The temperature distribution at t = 3 ms for the 2-step reaction model is shown in Fig. 23. These results are quite similar to the base case shown in Fig. 5 but the peak temperatures are significantly lower (3220 K for 2-step model vs. 4720 K for 1-step model). The peak pressure in the detonation front is only slightly lower with max value of 39.8 bar. The deflagration front is corrugated which is the effect of much violent detonation development after initiation. Also the boundary between the post-deflagration zone and post-detonation zone is more curved and the contact discontinuity quickly develops Kelvin-Helmholtz-like vortex structures. What is more the detonation wave velocity is equal to 1888 m/s so just 5.5% above theoretical CJ value. It is important to note that the omission of the correction factors allows for use of the "stiff" chemistry solver which accelerates computations as it allows for higher time step. Similar simulations with correction factors applied via Used Defined Functions (UDFs) enforce the use of direct solver for chemical source terms with smaller time step and associated round-off errors. For such case the detonation velocity is underestimated by 6.5%. Further test cases with this 2-step chemical reaction model will be run in the future. Once the lessons learned are collected and analyzed, more sophisticated models like Gerasimov [6, 7] or Strelkova [19] will be considered. Obviously, a higher computational cost should be expected (more species to track, more reactions and species source/sink rates to be calculated using the Arrhenius equation, which uses a computationally expensive "exp" function), but multi-step reaction models of

moderate size seem promising and worth testing in the future.

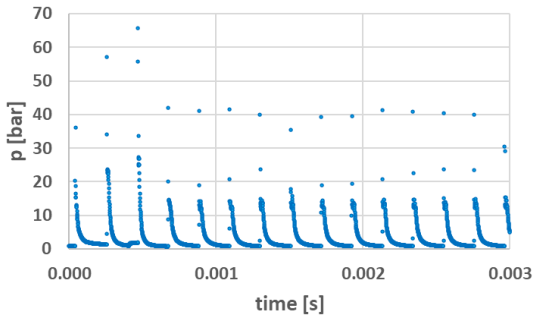

Fig. 18. History of pressure variation at "pressure gauge" for baseline case

3.5. Mesh sensitivity study

As it was mentioned before, the mesh used in these analyzes is quite coarse and higher mesh resolution may give more precise results. If the original mesh with cell size 0.5 × 0.5 mm is replaced by mesh with cells 62.5 × 62.5 μm then the resolution will increase 8 times but at the same time the cell count increases 64 times (8 × 8 = 64), and the time step will be reduced 8 times. For the uniformly refined mesh the overall computational cost would increase thus $8^3 = 512$ times requiring significantly bigger computational resources to obtain the results in the same time.

A partial solution for this problem is an application of the Adaptive Mesh Refinement (AMR) technique where only a small number of cells is refined ("adapted") to increase local resolution. Thus, the mesh sensitivity with AMR is also local but can be achieved in a reasonable time and with moderate resources. The cells to be adapted are selected based on user-defined criteria. Specifically, the gradients of the density (Schlieren-like), temperature, and fuel mass fraction indicate where the mesh should be refined to get better resolution of pressure, temperature, density, and fuel concentration. High gradients of these parameters are typically encountered in shock waves, flame fronts, and contact discontinuities. The specific numeric values of the criteria used for cell refinement and coarsening is obtained by trial and error as they are case-dependent.

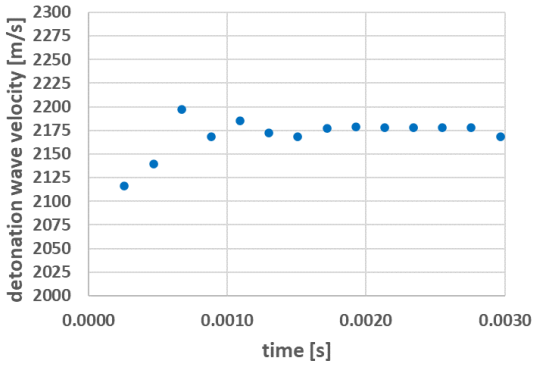

Fig. 19. Detonation wave velocity estimated based on history of pressure at "pressure gauge"

Figures 24–26 show the results of analysis for the base case where the mesh adaptation was turned on after 1 ms of physical time with 3 levels of refinement using non-scaled criteria summarized in Table 1. These criteria are case-dependent and strongly depend on users' judgment. Thus, they cannot be called "optimal," but they work well. It is important to note that mesh refinement is done when ANY of the conditions is fulfilled, while mesh coarsening is possible when ALL criteria are met at the same time.

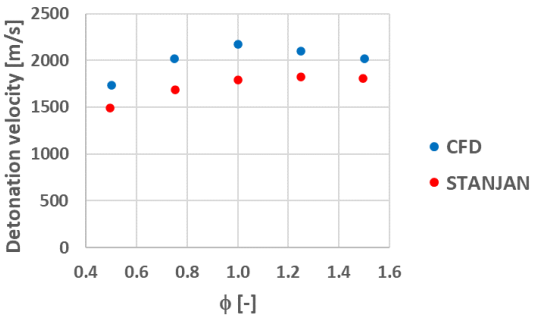

Fig. 20. Detonation wave velocity for kerosene-air mixture at inlet conditions of p = 1 bar, T = 300 K and equivalence ratios from ϕ = 0.5 to 1.5

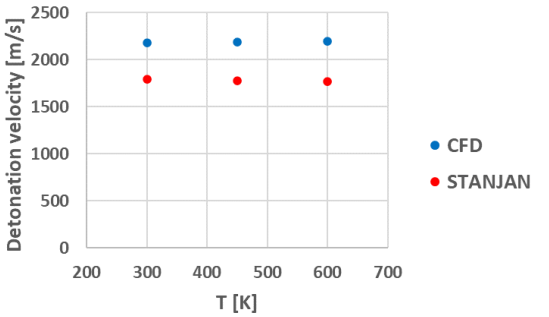

Fig. 21. Detonation wave velocity for kerosene-air mixture at inlet conditions of p = 1 bar, ϕ = 1.0, and temperatures T = 300 K, 400 K and 600 K

Table 1. Mesh adaption criteria (SI units)

Criterion	Mesh coarsening	Mesh refinement
Density gradient	< 0.025	> 0.100
Temperature gradient	< 100	> 200
Fuel gradient	< 0.0050	> 0.0075

At first, it may appear that the structure of the flow field is very similar to the structure shown in Fig. 5–7 with a much sharper view of detonation wave, contact discontinuity and shock wave, but there are distinct differences. First of all, the detonation wave is more curved, and the point of origin of the contact discontinuity and shock wave lags behind the center of the detonation wave. There is a fish-scale structure behind the detonation front, and the contact discontinuity develops Kelvin-Helmholtz-like vortex structure. The Kelvin-Helmholtz structure develops in the deflagration front, indicating an x-velocity gradient in this area, as well. The "reflected post-contact-discontinuity wave" is also visible in Fig. 26, but it does not propagate upstream as far as the coarse mesh case. It coincides with the point of origin of the contact discontinuity and shock wave and is diminished in the zone just downstream of it.

One can also include additional criteria for mesh adaptation based on y-velocity gradients or differences. The temperature distribution for this case is shown in Fig. 27 where better resolution of vortices in the deflagration front can be noticed. These vortices create another Kelvin-Helmholtz-

like vortex structure, but one more refinement level would probably be required to capture it precisely.

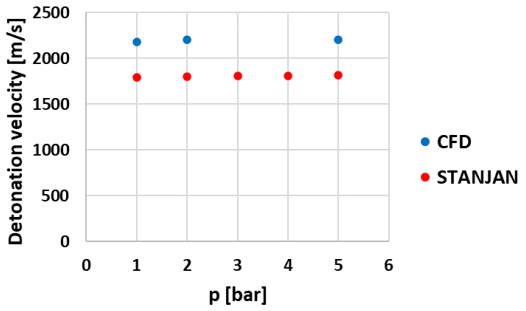

Fig. 22. Detonation wave velocity for kerosene-air mixture at inlet conditions of T = 300 K, ϕ = 1.0, and pressures p = 1 bar, 2 bar and 5 bar

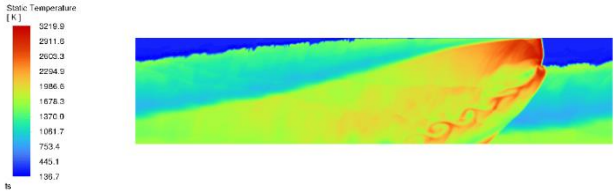

Fig. 23. Temperature distribution within the domain at t = 3 ms for the 2-step chemical reaction model

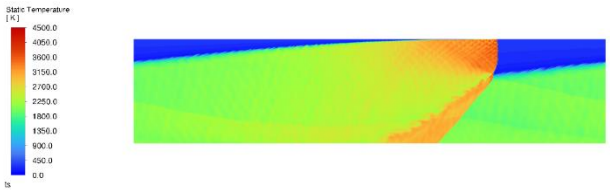

Fig. 24. Temperature distribution within the domain at t = 3 ms (AMR turned on)

Fig. 25. Pressure distribution within the domain at t = 3 ms (AMR turned on)

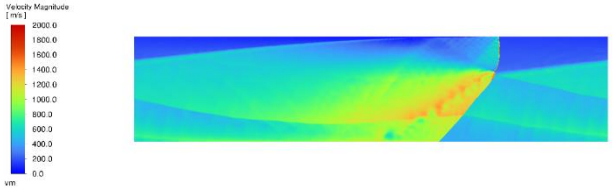

Fig. 26. Velocity magnitude distribution within the domain at t = 3 ms (AMR turned on)

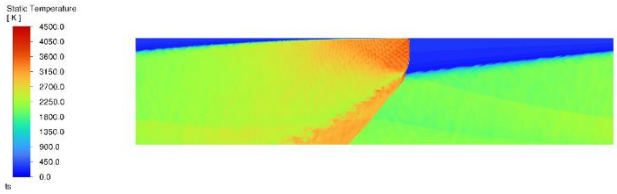

Fig. 27. Temperature distribution within the domain at t = 3.8 ms (AMR + adaptation on y-velocity gradient)

The zoom-ins into the detonation wave structure presented in Fig. 28–30 show more insight into the dynamics of the detonation front. One can notice that the fish-scale structure is the relic of the multiple small-scale triple-point motion and collisions, which are also responsible for the creation of smoke-foil records on the walls during detonation tests. The small bulges seen in Fig. 28–30 are expanding Mach stems, separated by triple points and incident shocks. The triple points propagate toward each other, collide and are the origins of new Mach stems, while the previous Mach stems weaken and become incident shocks. This process supports the forward motion of the detonation front. The detonation wave speed is only 0.77% lower than in the coarse mesh case. The adapted mesh is shown in Fig. 31.

The impact of the adaptation based on additional criterion y-velocity differences is shown in Fig. 32. Clearly it helps to resolve vortices within the contact discontinuity and deflagration front. The mesh coarsening was done for a local y-velocity difference (not gradient!) of < 200 and refinement for the y-velocity difference of > 500. Again, these numbers were obtained by trial and error.

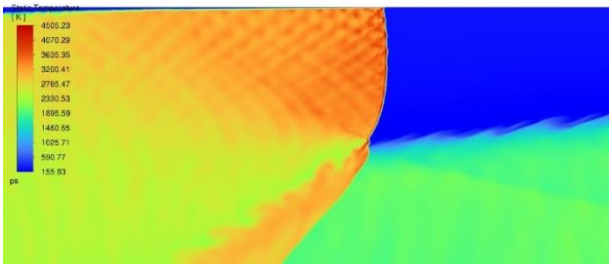

Fig. 28. Temperature distribution (zoom-in) in the detonation front at t = 3 ms

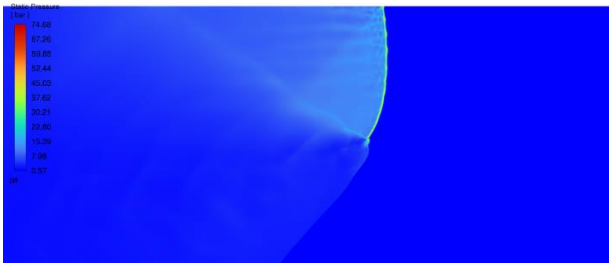

Fig. 29. Pressure distribution (zoom-in) in the detonation front at t = 3 ms

The experimentally observed detonation cell size is much larger than cells obtained in this analysis. The cell size in CFD analysis is very sensitive to the combustion model used in calculations. Specifically, the 2-step model of Frenzelli [5] does not predict the dynamics of the detonation front visible in Fig. 28–30. Figure 33 shows the temperature distribution in the detonation front for the 2-step reaction model, and there is no indication of triple point and Mach stems presence in the wave. It might be that the calculated time after the AMR was turned on was too short. Kohama [13] showed that detonation cell size can evolve for a very long time after initiation and that it may produce cells of different sizes at the same location of the detonation front. Another option is that the domain is too small and does not allow for the development of the cellular structure. The height of the detonation front depends on how far the

deflagration front moves downstream before it gets in contact with the detonation front. The latter depends on the distance to the proceeding wave (so itself), and finally, this depends on the width of the domain. Further analysis will be required to verify this hypothesis.

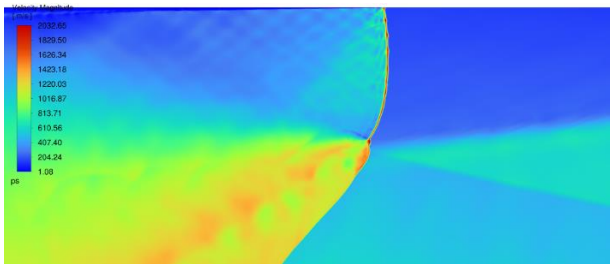

Fig. 30. Velocity magnitude distribution (zoom-in) in the detonation front at t = 3 ms

Nevertheless it is necessary to run such analyzes with high mesh resolution. The AMR technique is quite effective here. The mesh resolution was increased locally 8 times, while the overall cell count increased only 2 times. The 8-times shorter time step and 2-times larger mesh in this particular case were offset by the use of slightly larger computational resources than in the coarse-mesh case. Figure 31 shows details of the mesh in the detonation front. One can easily notice that the mesh is gradually refined in the detonation front, deflagration wave and shock wave. The contact discontinuity is not well refined indicating that the selected adaption criteria are not able to find this area.

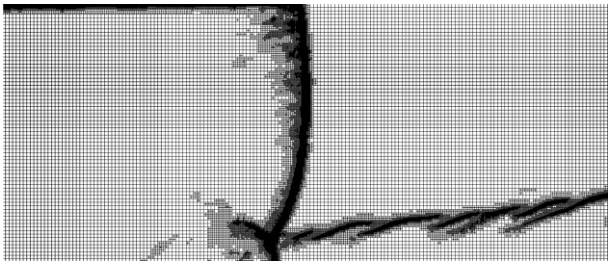

Fig. 31. Mesh density (zoom-in) in the detonation front at t = 3 ms

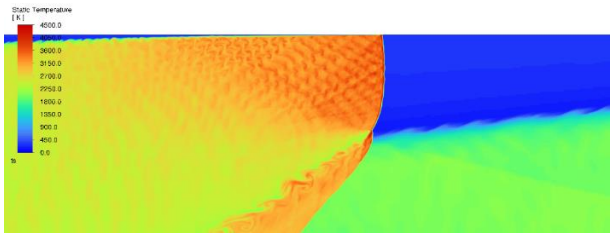

Fig. 32. Temperature distribution (zoom-in) in the detonation front at t = 3.8 ms (AMR + adaptation on y-velocity gradient)

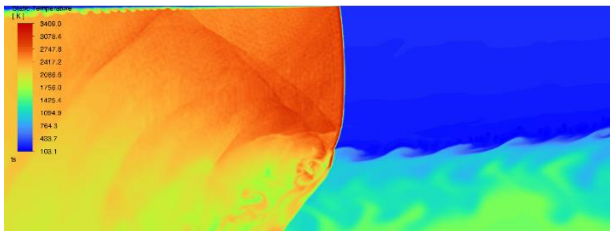

Fig. 33. Temperature distribution (zoom-in) in the detonation front at t = = 3.5 ms (2-step combustion model of Frenzelli [5], AMR + adaptation on y-velocity gradient)

4. Conclusions and future plans

The methodology of the RDE simulation presented in this paper is inherently associated with ANSYS Fluent, but it can be easily leveraged to any other software package (commercial, open source, or in-house codes). Its capability in the area of detonation research makes it an effective tool in support of R&D activities required for the development of efficient aviation propulsion systems. Its flexibility allows one to concentrate on the problem to be solved and removes almost all the burden associated with computer code development. Even though it has some limitations, it helps to analyze physical processes occurring in propagating detonation front and reproduce phenomena observable in real detonations.

The 2D model is suitable for methodology development but it cannot be used for model assessment as there is no practical linear RDE with periodic boundary conditions that could provide experimental data for comparison with CFD. For model assessment, a 3D case is required with geometry representing test hardware.

The 2D simulations for a gaseous mixture of kerosene vapor and air presented in this paper indicate that:

- the 1-step global combustion model reproduces the trends of the detonation wave velocity vs. equivalence ratio with consistent overprediction of the wave speed by ~21% (see Fig. 34)
- the 2-step combustion model provides much better agreement with the theoretical speed of the detonation wave (from –6.5% to +5.5%) (Fig. 34)
- the structure of the detonation wave is consistent with similar results available in the literature with addition of an upstream propagating wave caused by the reflection of the main wave structure from the outlet boundary condition
- the simplified approach to boundary conditions modelling works reasonably well but the initial fuel and oxidizer mixing process is omitted while it can be actually important to the development and stability of the detonation wave propagation
- the initiation method represents strong initiator and is effective in quickly starting the detonation
- a sufficiently small mesh cell size is critical to obtain details of the detonation wave structure, including cellular structure and Kelvin-Helmholtz vortex structures
- the Adaptive Mesh Refinement method allows for capture of the fine features of the flow field with reasonable computational cost
- the criteria for mesh refinement and coarsening are subjective and chosen by trial and error, but are an efficient tool to find balance between resolution of the model, required computational resources and computer simulation time.

The aforementioned results allow for an extension of this methodology and its application to more demanding problems. Specifically, further research will include:

- application of multi-step combustion models and inclusion of radicals like CO and OH
- extension to the full set of Navier-Stokes equations
- 3D models of generic and realistic geometries and methodology assessment against test data

– addition of an inlet zone where fuel and air can mix prior to combustion
– addition of exit nozzle
– extension of the model to heterogeneous mixtures (liquid fuel droplets in air).

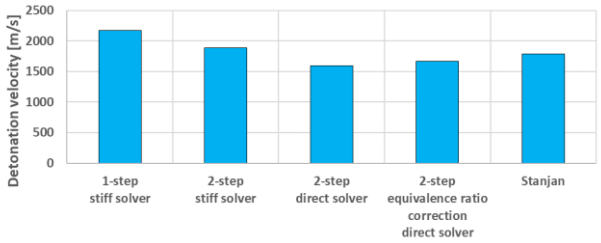

Fig. 34. Comparison of detonation wave velocity for different combustion models and solver settings

It must be noted that the experimental campaigns conducted at the Łukasiewicz Network – Institute of Aviation in the past (Wolański [24], Perkowski [17], Kindracki [11] and Kawalec [9]) resulted in the first launch of the experimental rocket powered by liquid-fueled Continuous Rotating Detonation Rocket Engine (CRDRE) (Kawalec [10]). The fuel (liquid propane) and oxidizer (liquid nitrous oxide) were carried on board of the rocket. The tests are being continued nowadays with a focus on air-breathing RDE combustion chambers of various designs supplied with a more convenient propellant: classical aviation Jet-A fuel. It should be much easier to find practical applications for such designs, for example, in future supersonic aircraft. The most promising configurations will be modelled in ANSYS Fluent to get a better insight into the processes taking place within these engines.

It is expected that the ANSYS tools and the modelling methodology will contribute to the development of an efficient propulsion system utilizing the rotating detonation phenomena.

Acknowledgements

The author gratefully acknowledges Polish high-performance computing infrastructure PLGrid (HPC Center: ACK Cyfronet AGH) for providing computer facilities and support within computational grants no. PLG/2022/015697 and PLG/2023/016677. The author also wants to express his gratitude to Ms. Elżbieta Zocłońska and Mr. Maksymilian Augustyn of the Łukasiewicz Research Network – Institute of Aviation, Poland, and Dr. Maciej Szudarek of Symkom – ANSYS Channel Partner, for their help in model development and testing.

Nomenclature

A	pre-exponential factor
AMR	adaptive mesh refinement
c_{pi}	i-th specie specific heat at constant pressure
CFD	computational fluid dynamics
CJ	Chapman-Jouguet point
CRDE	continuous rotating detonation engine
CRDRE	continuous rotating detonation rocket engine
DDT	deflagration-to-detonation transition
E	total specific energy of the mixture
E_A	activation energy
F, G	vectors of fluxes
GUI	graphical user interface
k	reaction rate
L	domain length (y direction)
M	molar mass of the mixture
$M_{C_{12}H_{23}}$	molar mass of kerosene
n	number of species
p	static pressure
Q	vector of source terms
R	universal gas constant
R&D	research and development
RDE	rotating detonation engine
Roe-FDS	Roe flux-difference splitting scheme
SAF	sustainable aviation fuel
SI	international standard units
T	static temperature of the mixture
TRL	technology readiness level
u	velocity component in x direction
U	vector of variables
UDF	user-1ined function
v	velocity component in y direction
W	domain width (x direction)
y_i	i-th specie mass fraction
ρ	mixture density
ρ_i	i-th specie density, i = 1, …, n
ϕ	equivalence rati
$\dot{\omega}_i$	the i-th specie source term
[…]	molar concentration of species

Bibliography

[1] ANSYS Fluent Theory Guide, https://ansys.com. https://ansyshelp.ansys.com/public/account/secured?returnurl=////Views/Secured/corp/v232/en/flu_th/flu_th.html

[2] Dagaut P, Cathonnet M. The ignition, oxidation, and combustion of kerosene: a review of experimental and kinetic modelling. Prog Energ Combust. 2006;32(1):48-92. https://doi.org/10.1016/j.pecs.2005.10.003

[3] Davidenko DM, Gökalp I, Kudryavtsev AN. Numerical 14dy of the continuous detonation wave rocket engine. 15th AIAA International Space Planes and Hypersonic Systems and Technologies Conference. 28 April–1 May 2008, Dayton. Ohio, AIAA 2008-2680. https://doi.org/10.2514/6.2008-2680

[4] Dziemińska E, Fukuda M, Hayashi AK, Yamada E. Fast flame propagation in hydrogen-oxygen mixture. Combust Sci Technol. 2012;184(10-11):1608-1615. https://doi.org/10.1080/00102202.2012.695252

[5] Franzelli B, Riber E, Sanjosé M, Poinsot T. A two-step chemical scheme for kerosene-air premixed flames. Combust Flame. 2010;157:1364-1373. https://doi.org/10.1016/j.combustflame.2010.03.014

[6] Gerasimov GY, Levashov VY. Kinetic models of combustion of kerosene. Journal of Engineering Physics and Thermophysics. 2024;97:506-524. https://doi.org/10.1007/s10891-024-02918-x
[7] Gerasimov GY, Tunik YV, Kozlov PV Simplified kinetic model of kerosene combustion. Russ J Phys Chem B. 2021; 15:637-644. https://doi.org/10.1134/S1990793121040163
[8] Hishida M, Fujiwara T, Wolanski P. Fundamentals of rotating detonations. Shock Waves. 2009;19:1-10. https://doi.org/10.1007/s00193-008-0178-2
[9] Kawalec M, Perkowski W, Wolanski P. Development of rocket engines with detonation combustion chamber. In: Research on detonative propulsion in Poland. Institute of Aviation Scientific Publication. 2021;60:163-181.
[10] Kawalec M, Perkowski W, Łukasik B Applications of the continuously rotating detonation to combustion engines at the Łukasiewicz – Institute of Aviation. Combustion Engines. 2022;191(4):51-57. https://doi.org/10.19206/CE-145409
[11] Kindracki J, Wolański P, Gut Z. Experimental research on the rotating detonation in gaseous fuels–oxygen mixtures. Shock Waves. 2011;21:75-84. https://doi.org/10.1007/s00193-011-0298-y
[12] Knowlen C, Mundt T, Kurosaka M. Experimental results for 25-mm and 51-mm rotating detonation rocket engine combustors. Shock Waves. 2023;33:237-252. https://doi.org/10.1007/s00193-023-01120-x
[13] Kohama S, Ito T, Tsuboi N, Ozawa K, Hayashi AK. Two-dimensional detailed numerical simulation of ammonia/hydrogen/air detonation: hydrogen concentration effects and transverse detonation wave structure. Shock Waves. 2024;34:139-154. https://doi.org/10.1007/s00193-024-01181-6
[14] Kublik D, Kindracki J, Wolański. Evaluation of wall heat loads in the region of detonation propagation of detonative propulsion combustion chambers. Appl Therm Eng. 2019; 156:606-618. https://doi.org/10.1016/j.applthermaleng.2019.04.084
[15] Meyer SJ, Polanka MD, Schauer F, Anthony RJ, Stevens CA, Hoke J, Rein KD. Experimental Characterization of Heat Transfer Coefficients in a Rotating Detonation Engine, 55th AIAA Aerospace Sciences Meeting. 2017. https://doi.org/10.2514/6.2017-1285
[16] Nishimura J Experimental Research on a long-duration operation of a rotating detonation engine. In: Sasoh A, Aoki T, Katayama M (eds). 31st International Symposium on Shock Waves 2 (ISSW 2017). Springer 2019. https://doi.org/10.1007/978-3-319-91017-8_15
[17] Perkowski W, Bilar A, Augustyn M, Kawalec M. Air-breathing rotating detonation engine supplied with liquid kerosene: propulsive performance and combustion stability. Shock Waves. 2024;34:181-192. https://doi.org/10.1007/s00193-024-01185-2
[18] Reynolds WC. The element potential method for chemical equilibrium analysis: Implementation in the interactive program STANJAN, version 3. Technical Rept., 1986.
[19] Strelkova MI, Kirillov IA, Potapkin BV, Safonov AA, Sukhanov LP, Umanskiy S. Detailed and reduced mechanisms of a jet combustion at high temperatures. Combust Sci Technol. 2008;180(10-11):1788-1802. https://doi.org/10.1080/00102200802258379
[20] Tingas E-A (ed.). Hydrogen for future thermal engines, green energy and technology. Springer Nature Switzerland AG 2023. https://doi.org/10.1007/978-3-031-28412-0
[21] Westbrook CK, Dryer FL. Chemical kinetic modelling of hydrocarbon combustion. Prog Energ Combust. 1984;10(1): 1-57. https://doi.org/10.1016/0360-1285(84)90118-7
[22] Wolański P. Detonation engines. Journal of KONES. 2011; 18(3):515-521.
[23] Wolański P. Detonative propulsion. Proceedings of Combustion Institute. 2013;34(1):125-158. https://doi.org/10.1016/j.proci.2012.10.005
[24] Wolański P. RDE research and development in Poland. Shock Waves. 2021;31:623-636. https://doi.org/10.1007/s00193-021-01038-2
[25] Wolanski P (ed.). Research on detonative propulsion in Poland. Institute of Aviation Scientific Publication. 2021;60.
[26] NASA's Marshall Space Flight Center YouTube official channel. https://30.youtube.com/watch?v=UShD03eG9IU
[27] Xie Q, Ji Z, Wen H, Ren Z, Wolański P, Wang B. Review on the rotating detonation engine and it's typical problems. Transactions on Aerospace Research. 2020;2020(4):107-163. https://doi.org/10.2478/tar-2020-0024
[28] Yi TH, Lou J, Turangan CK, Wolanski P. Numerical study of detonation process in rotating detonation engine and its propulsive performance. In: Research on detonative propulsion in Poland. Institute of Aviation Scientific Publication. 2021;60:79-91.
[29] Zeng W, Liang S, Li HX, Ma HA. Chemical kinetic simulation of kerosene combustion in an individual flame tube. Journal of Advanced Research. 2014;5(3):357-366. https://doi.org/10.1016/j.jare.2013.06.002
[30] Zettervall N, Fureby C, Nilsson EJK. A reduced chemical kinetic reaction mechanism for kerosene-air combustion. Fuel. 2020;269:117446. https://doi.org/10.1016/j.fuel.2020.117446
[31] Zhou J, Song F, Xu S, Yang X, Zheng Y. Investigation of rotating detonation fueled by liquid kerosene. Energies. 2022;15:4483. https://doi.org/10.3390/en15124483

Krzysztof Benkiewicz, PhD. – Łukasiewicz Research Network – Institute of Aviation, Poland.
e-mail: *krzysztof.benkiewicz@ilot.lukasiewicz.gov.pl*